PERGAMON

Journal of Quantitative Spectroscopy & Radiative Transfer 63 (1999) 393–407

Journal of Quantitative Spectroscopy & Radiative Transfer

www.elsevier.com/locate/jqsrt

The dependence of the radiative characteristics of optically thick media on the shape of particles

Alexander A. Kokhanovsky[a,b,*], Andreas Macke[c]

[a]*IMVT/UVT, Technical University Clausthal, Leibnizstrasse 19, D-38678 Clausthal-Zellerfeld, Germany*
[b]*Institute of Physics, 70 Skarina Avenue, Minsk 220072, Belarus*
[c]*Institute of Oceanology, Duesternbrooker Weg 20, D-24105 Kiel, Germany*

This paper is dedicated to Professor A.P. Ivanov on the occasion of his 70th birthday

Abstract

The aim of this paper is to study the dependence of reflection, absorption, and transmission of light by optically thick, weakly absorbing disperse media on the shape of constituent particles. Single scattering by nonspherical particles is calculated in the framework of the Rayleigh and geometrical optics approximations. The ratio of the average volume to the average surface of particles and their volumetric concentration are kept constant. Thus, the extinction coefficient and the optical thickness of different media under consideration are the same. Calculations are performed for ice particles at wavelengths of 0.645, 1.24, 1.64, and 2.13 μm. The respective refractive indices range from $1.3082–i1.325\times10^{-8}$ (weak absorption) to $1.2674–i5.65\times10^{-4}$ (moderate absorption). The radiative characteristics are calculated in the framework of approximate analytical formulae valid for optically thick, weakly absorbing media.

1. Introduction

Studies of the influence of the shape of aerosol and cloud particles on their optical properties are important for many applications in climate modelling [1], remote sensing [2,3], optical particle sizing [4], and spectroscopy of disperse media [5]. It follows from general considerations that this influence can often be neglected for particles that are much smaller than the wavelength of the incident radiation ($a \ll \lambda/|m|$, where a is the particle size, λ is the wavelength, and $m = n - \mathrm{i}\chi$ is the

* Corresponding address: Stepanov Institute of Physics, National Academy of Sciences, Skarina Avenue 68, 220072 Minsk, Byelorussia. Tel.: + 375-172-841997; fax: + 375-172-840879

E-mail address: a.kokhanovsky@ieee.org (A.A. Kokhanovsky)

0022-4073/99/$ - see front matter
PII: S0022-4073(99)00027-8

particle refractive index). However, this is not the case for large ($a \gg \lambda$) scatterers. For instance, Takano and Liou [6] demonstrated that neither area-equivalent nor volume-equivalent spheres can adequately approximate large hexagonal cylinders in terms of their single scattering and absorption properties. The same is true for circular cylinders and spheroids [3,7].

Differences in radiative characteristics of multiple-scattering media consisting of spherical and nonspherical particles are less pronounced than for single-scattering characteristics. This is due to the randomization of photon directions in the course of many scattering events. The investigation of the influence of crystal shapes on the radiative fluxes at visible wavelengths was performed by many authors [8–12]. Numerical solutions of the radiative transfer equation were used in these studies. It was found that the differences in radiative fluxes of media consisting of spherical and nonspherical particles decrease with increasing optical thickness τ.

The aim of this paper is to investigate the influence of particle nonsphericity on radiative fluxes in plane-parallel layers with large optical thicknesses ($\tau \geq 7$). This allows us to use simple asymptotic equations for the radiative characteristics [13,14]. We consider Rayleigh ($a \ll \lambda$) and large ($a \gg \lambda$) particles. The following shapes of randomly oriented scatterers are studied in the framework of the ray optics approximation [15,16]: spheres (s), prolate spheroids (ps), oblate spheroids (os), circular columns (cc), circular plates (cp), hexagonal columns (hc), and hexagonal plates (hp). The ratio of the volume to the surface area of the particles is kept constant. Calculations for ice particles are performed at wavelengths $\lambda = 0.645, 1.24, 1.64$, and $2.13\ \mu$m.

2. Single-scattering characteristics

2.1. Rayleigh scatterers

For Rayleigh scatterers ($a \ll \lambda/|m|$), the absorption cross section C_{abs} is proportional to the particle volume V ($C_{\text{abs}} = \alpha V$) and the scattering cross section C_{sca} is proportional to the particle squared volume V^2 ($C_{\text{sca}} = \beta V^2$). Furthermore, the phase function $p(\theta) = 0.75(1 + \cos^2\theta)$ does not depend on the particle shape and size. In the case of soft particles ($m \to 1$), the dependence of the constants α and β on the particle shape is negligible. In general, α and β depend on the shape of the particles and on their refractive index m [17]. For example, for randomly oriented ellipsoids we have [17–19]:

$$\alpha = f_1(n)\gamma, \tag{1}$$

$$\beta = f_2(n)k^4, \tag{2}$$

where

$$f_1(n) = \frac{n}{3}\sum_{j=1}^{3}\frac{1}{(1+\upsilon L_j)^2 + (\mu L_j)^2}, \tag{3}$$

$$f_2(n) = \frac{1}{18\pi}\sum_{j=1}^{3}\frac{(\upsilon + (\upsilon^2+\mu^2)L_j)^2 + \mu^2}{[(1+\upsilon L_j)^2 + \mu^2 L_j^2]^2}, \tag{4}$$

and $\upsilon = n^2 - 1 - \chi^2$, $\mu = 2n\chi$, $k = 2\pi/\lambda$, $\gamma = 4\pi\chi/\lambda$. L_j are called geometrical factors [17]. The absorption coefficient χ is small for many substances in the visible region of the electromagnetic spectrum and Eqs. (3) and (4) simplify in this particular case as well:

$$f_1(n) = \frac{n\psi}{3}, \qquad f_2(n) = \frac{(n^2-1)^2}{18\pi}\psi, \tag{5}$$

where

$$\psi = \sum_{j=1}^{3} [1 + (n^2 - 1)L_j]^{-2}. \tag{6}$$

The relative errors Δ_1 and Δ_2 of the absorption and scattering cross sections due to neglecting the nonspherical shape of particles,

$$\Delta_1 = \frac{f_1^{\mathrm{n}} - f_1^{\mathrm{s}}}{f_1^{\mathrm{s}}}, \qquad \Delta_2 = \frac{f_2^{\mathrm{n}} - f_2^{\mathrm{s}}}{f_2^{\mathrm{s}}} \tag{7}$$

coincide in this particular case. They are equal to (see Eq. (6))

$$\Delta = \frac{\psi^{\mathrm{n}} - \psi^{\mathrm{s}}}{\psi^{\mathrm{s}}}, \tag{8}$$

where indices n and s denote quantities for nonspherical and spherical shapes, respectively. For instance, for prolate spheroids with semi-axes r, b, and l ($r = b < l$), it follows [19] that

$$L_1 = \left[1 + \frac{1-\varepsilon^2}{2\varepsilon^3}\ln\frac{1+\varepsilon}{1-\varepsilon} - \frac{1}{\varepsilon^2}\right], \qquad L_2 = \frac{1-L_1}{2}, \qquad L_3 = \frac{1-L_1}{2}, \tag{9}$$

where $\varepsilon = \sqrt{1-\xi^2}$ and $\xi = r/l$. For small values of ε we have:

$$\ln\frac{1+\varepsilon}{1-\varepsilon} = 2\left(\varepsilon + \frac{\varepsilon^3}{3} + \frac{\varepsilon^5}{5} + \cdots\right), \tag{10}$$

and

$$L_1 = \frac{1}{3} - \frac{2\varepsilon^2}{15}. \tag{11}$$

The geometrical factors for spheres ($\varepsilon = 0$) are $L_1 = L_2 = L_3 = \frac{1}{3}$. Thus, L_1 for spheroids is always smaller than that for spheres. For a given value of ε, the geometrical factors for oblate spheroids (and, thus, the light scattering characteristics) are closer to the respective values for spherical particles than those for prolate spheroids [19].

For soft particles ($m \to 1$) at $\chi/n \ll 1$, it follows that $f_1(n) \to 1$, $f_2(n) \to (2/3\pi)|m-1|^2$ regardless of their shape. In this particular case only the particle volume is important. This is approximately true even for comparatively large refractive indices such as those of ice ($n = 1.31$) and dust ($n = 1.52$) at visible wavelengths (see Fig. 1). Thus, single light scattering characteristics of small nonspherical ($a \ll \lambda/|m|$) particles can be approximately represented by those of volume-equivalent spheres. It

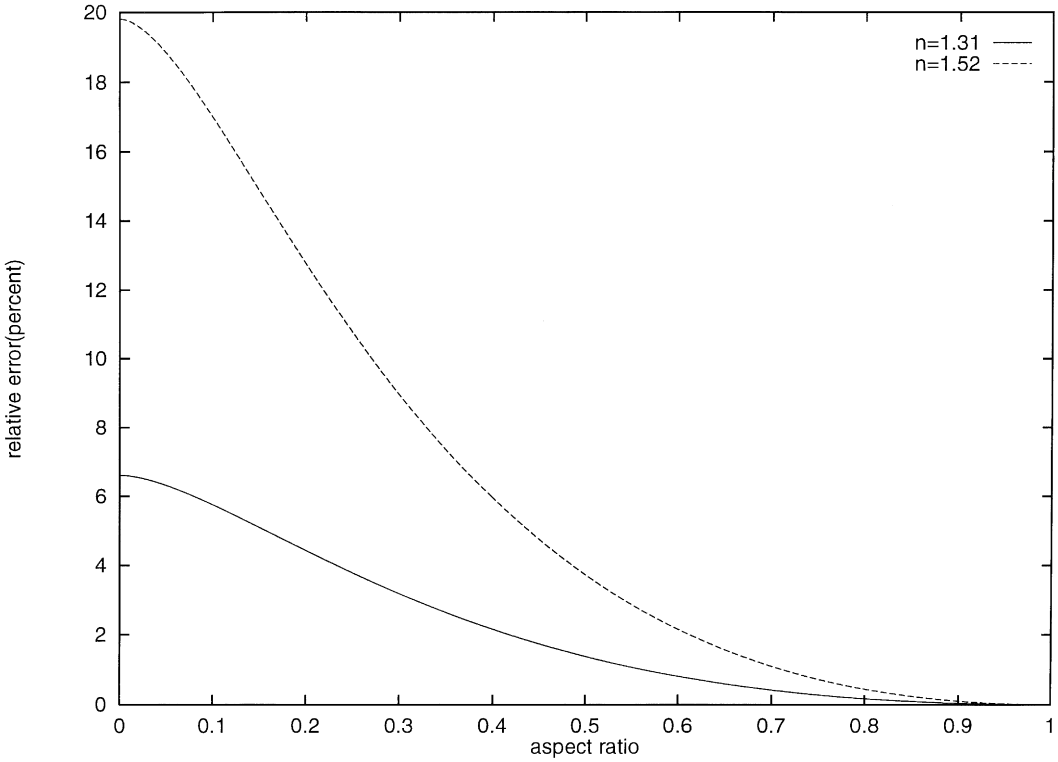

Fig. 1. Dependence of the relative error Δ [see Eqs. (8), (16), and (9)] on the aspect ratio ξ for Rayleigh ice ($n = 1.31$) and dust ($n = 1.53$) prolate spheroids in random orientation.

appears that the same is true [1] even for larger particles ($a \leq 5\lambda$), but only with respect to the integral light scattering characteristics, namely the single scattering albedo $w_0 = 1 - (\sigma_{abs}/\sigma_{ext})$ (σ_{abs} and σ_{ext} are the extinction and absorption coefficients), the extinction coefficient σ_{ext}, and the asymmetry parameter $g = \frac{1}{2}\int_0^\pi p(\theta)\sin\theta\cos\theta\,d\theta$. According to the similarity principle [13], the radiative fluxes and albedos of scattering media depend mostly on the parameters $s = \sqrt{(1-\omega_0)/3(1-g)}$ and $\tau(1-g)$. Thus, volume-equivalent spheres can be used to model the radiative fluxes of scattering layers with small to moderately sized particles. Of course, such a substitution is not possible if one needs to estimate polarization characteristics or bidirectional reflectances of a layer consisting of nonspherical particles [8–12,20].

2.2. Large convex particles

The restrictions on the particle size and refractive index that will be considered now are as follows: $x \gg 1$, $2x|m-1| \gg 1$, where $x = 2\pi a_m/\lambda$, a_m is the minimal dimension of a convex particle. It is assumed that particles are monodisperse and randomly oriented. The extinction coefficient σ_{ext} for such large convex particles in random orientation can be found from the following

Table 1
Volume V, surface area Σ, and effective radius $a_{ef} = 3V/\Sigma$ for particles of different shapes

Type of a particle	V	Σ	a_{ef}
Sphere (a – radius)	$4\pi a^3/3$	$4\pi a^2$	a
Prolate spheroid ($b = r < l$ are semi-axes, $\varepsilon = \sqrt{1-\xi^2}$, $\xi = r/l$)	$(4\pi/3)r^2 l$	$4\pi r^2\left[\frac{1}{2} + \frac{\arcsin\sqrt{1-\xi^2}}{2\xi\sqrt{1-\xi^2}}\right]$	$\frac{2r}{\xi + (\arcsin\sqrt{1-\xi^2}/\sqrt{1-\xi^2})}$
Oblate spheroid ($b = r > l$ are semi-axes, $\varepsilon' = \sqrt{\xi^2-1}$, $\xi = r/l$)	$(4\pi/3)r^2 l$	$4\pi r^2\left[1 + \frac{\ln(1+\varepsilon')/(1-\varepsilon')}{2\xi^2\varepsilon'}\right]$	$\frac{r}{\xi + \frac{\ln((1+\varepsilon')/(1-\varepsilon'))}{2\xi\varepsilon'}}$
Circular cylinder (l is the length, r is the radius, $\xi = r/l$)	$\pi r^2 l$	$2rl(1+\pi\xi)$	$3\pi r/2(1+\pi\xi)$
Hexagonal cylinder (l is the length, r is the side of the cross section, $\xi = r/l$)	$\sqrt{3}r^2 l/2$	$6rl(1+(\xi/2\sqrt{3}))$	$\frac{\sqrt{3}r}{4(1+(\xi/2\sqrt{3}))}$

equation [7]:

$$\sigma_{ext} = \frac{1.5c}{a_{ef}}, \tag{12}$$

where $a_{ef} = 3V/\Sigma$ is the effective radius, V is the volume of a particle, Σ is the surface area, and c is the volumetric concentration. For spheres with radius a, the value of a_{ef} is equal to a. Thus, it follows that in the case of large nonspherical particles the appropriate effective radius (at least for the calculation of the extinction coefficient and optical thickness $\tau = \sigma_{ext} l$, where l is the geometrical depth) could be the radius defined via the ratio of the average volume and surface area of particles. Extinction coefficients of spherical and large nonspherical convex particles in random orientation with the same values of a_{ef} and c coincide.

To check the applicability of a common effective radius to other light scattering characteristics, we have calculated the single scattering albedo ω_0, the asymmetry parameter g, and the similarity parameter $s = \sqrt{(1-\omega_0)/3(1-g)}$ for particles of different shapes by means of the geometrical optics approximation [15,16]. The ratio V/Σ was kept constant ($a_{ef} = 100\ \mu m$). The types of particles together with the correspondent definitions of V, Σ, and $a_{ef} = 3V/\Sigma$ are presented in Table 1. The corresponding geometrical dimensions are shown in Table 2.

Table 2
Parameters of particles used in calculations ($b = r$ and l are semi-axes of spheroids, l is the length of a hexagonal or a circular cylinder, r is the side of the hexagonal cross section or the radius of a circular cylinder)

Type of a particle	Sizes	The shape parameter
Sphere (S)	$a = 100$ μm	1
Prolate spheroid (PS)	$r = 85.46$ μm, $l = 170.92$ μm	2
Oblate spheroid (OS)	$r = 138.02$ μm, $l = 69.01$ μm	2
Hexagonal column (HC)	$r = 93.65$ μm, $l = 374.59$ μm	4
Hexagonal plate (HP)	$r = 143.65$ μm, $l = 143.65$ μm	1
Circular column (CC)	$r = 83.33$ μm, $l = 333.33$ μm	4
Circular plate (CP)	$r = 133.33$ μm, $l = 133.33$ μm	1

Table 3
Wavelengths λ, refractive indices of ice $m = n - i\chi$, and attenuation parameters p used in calculations

λ, μm	n	χ	p
0.645	1.3082	1.325e − 8	5.1629e − 5
1.24	1.2972	1.220e − 5	2.4727e − 2
1.64	1.2881	2.670e − 4	4.0917e − 1
2.13	1.2674	5.650e − 4	6.6667e − 1

The shape parameter in Table 2 is defined as the ratio of the largest to the smallest particle dimensions.

The wavelengths, refractive indices $m = n - i\chi$, and attenuation parameters $p = 2a_{ef}\gamma$ with $\gamma = 4\pi\chi/\lambda$, $a_{ef} = 100$ μm are presented in Table 3. The wavelengths selected are almost free of gaseous absorption and correspond to channels 1, 5, 6, and 7 of the Moderate Resolution Imaging Spectroradiometer (MODIS) on board of the NASA's Earth Observing System satellites.

One can see that the attenuation parameter p is smaller than 1 in our calculations. Large absorption is not of interest for this study because in this case ω_0 and g for spheres and randomly oriented nonspherical convex particles coincide [17]. The geometric optics results for the co-asymmetry parameter $1 - g$, the co-single scattering albedo $1 - \omega_0$, and the similarity parameter s are presented in Table 4.

First of all it follows that $1 - g$ and $1 - \omega_0$ differ considerably for spherical and nonspherical particles with the same effective radius a_{ef}. Thus, in agreement with previous work on this subject [8–12], it is not possible to substitute nonspherical particles by V/Σ-equivalent spheres for calculations of the single scattering characteristics. This was demonstrated in our earlier papers [3,7] as well. For instance, for hexagonal plates at $\lambda = 0.645$ μm, $1 - g$ is about two times larger than that for spheres. The probability of photon absorption by spheres $b = 1 - \omega_0$ is about 1.5 times smaller than that by hexagonal columns.

Table 4
Dependence of values of $1-g$, $1-\omega_0$, and $s=\sqrt{(1-\omega_0)/3(1-g)}$ on the type of particles (see Table 2) for different wavelengths λ and $a_{ef}=100$ μm

Shape	λ, μm	$1-g$	$1-\omega_0$	s
S	0.645	1.069 E − 1	2.158 E − 5	8.203 E − 3
PS	0.645	1.340 E − 1	2.497 E − 5	7.888 E − 3
OS	0.645	1.718 E − 1	2.611 E − 5	7.118 E − 3
HC	0.645	1.861 E − 1	3.028 E − 5	7.364 E − 3
HP	0.645	2.004 E − 1	2.921 E − 5	6.969 E − 3
CC	0.645	1.603 E − 1	2.646 E − 5	7.418 E − 3
CP	0.645	1.738 E − 1	2.635 E − 5	7.108 E − 3
S	1.24	1.016 E − 1	1.016 E − 2	1.827 E − 1
PS	1.24	1.261 E − 1	1.164 E − 2	1.754 E − 1
OS	1.24	1.610 E − 1	1.214 E − 2	1.585 E − 1
HC	1.24	1.743 E − 1	1.398 E − 2	1.635 E − 1
HP	1.24	1.902 E − 1	1.349 E − 2	1.537 E − 1
CC	1.24	1.517 E − 1	1.237 E − 2	1.649 E − 1
CP	1.24	1.660 E − 1	1.233 E − 2	1.574 E − 1
S	1.64	8.045 E − 2	1.398 E − 1	7.610 E − 1
PS	1.64	8.678 E − 2	1.507 E − 1	7.609 E − 1
OS	1.64	1.098 E − 1	1.559 E − 1	6.880 E − 1
HC	1.64	1.166 E − 1	1.696 E − 1	6.963 E − 1
HP	1.64	1.355 E − 1	1.671 E − 1	6.410 E − 1
CC	1.64	1.084 E − 1	1.584 E − 1	6.980 E − 1
CP	1.64	1.246 E − 1	1.609 E − 1	6.560 E − 1
S	2.13	6.584 E − 2	2.056 E − 1	1.024 E + 0
PS	2.13	6.593 E − 2	2.517 E − 1	1.044 E + 0
OS	2.13	8.105 E − 2	2.215 E − 1	9.545 E − 1
HC	2.13	8.833 E − 2	2.342 E − 1	9.401 E − 1
HP	2.13	1.066 E − 1	2.338 E − 1	8.549 E − 1
CC	2.13	8.424 E − 2	2.246 E − 1	9.427 E − 1
CP	2.13	9.828 E − 2	2.289 E − 1	8.810 E − 1

For all cases used in this study, $1-g$ and $1-\omega_0$ are the smallest for spherical particles. Therefore, spheres are characterized by smaller absorption and less isotropic phase functions in comparison with V/Σ-equivalent convex nonspherical particles (at least for shape parameters $\eta \leq 4$; see Table 2). This is not the case for extremely elongated or flattened particles [7]. However, small to moderate deviations from sphericity (which are widely encountered) should produce this result in general. The largest differences in absorption are found between spherical and hexagonal particles, the smallest differences are between spheres and spheroids. Cylinders occupy the intermediate place.

The values of $1-g$ and $1-\omega_0$ vary considerably for different particle shapes at $a_{ef}=const.$ However, the variation of the similarity parameter $s=\sqrt{(1-\omega_0)/3(1-g)}$ is small (see Table 4). It remains the same within 10% for all shapes considered (at $\lambda=const.$). The similarity parameter determines the spherical albedo of semi-infinite turbid media [13,14]. The larger values of s for spheres (see Table 4) imply smaller albedos.

3. Radiative characteristics of optically thick layers

In order to study the influence of different particle shapes on the radiative characteristics of turbid layers, we make use of the single scattering results shown in Table 4. The radiative characteristics are calculated with approximate equations for weakly absorbing ($s < 0.2$), optically thick ($\tau > 7$) layers. These equations are derived in the framework of the radiative transfer theory [13,14,21]. They are presented in Table 5 for the plane albedo $R(\mu_0)$, the spherical albedo R, the transmittance $T(\mu_0)$, the global transmittance T, and the global absorptance $A = 1 - R - T$. Here μ_0 is the cosine of the solar zenith angle. The accuracy of the formulae in Table 5 was discussed by Zege et al. [21]. The functions in Table 5 are defined as follows:

$$R(\mu_0) = \frac{1}{\pi} \int_0^1 \mu \, \mathrm{d}\mu \int_0^{2\pi} R(\mu, \mu_0, \psi) \, \mathrm{d}\psi, \tag{13}$$

$$R = \frac{2}{\pi} \int_0^1 \mu \, \mathrm{d}\mu \int_0^1 \mu_0 \, \mathrm{d}\mu_0 \int_0^{2\pi} R(\mu, \mu_0, \psi) \, \mathrm{d}\psi, \tag{14}$$

$$T(\mu_0) = \frac{1}{\pi} \int_0^1 \mu \, \mathrm{d}\mu \int_0^{2\pi} T(\mu, \mu_0, \psi) \, \mathrm{d}\psi, \tag{15}$$

$$T = \frac{2}{\pi} \int_0^1 \mu \, \mathrm{d}\mu \int_0^1 \mu_0 \, \mathrm{d}\mu_0 \int_0^{2\pi} T(\mu, \mu_0, \psi) \, \mathrm{d}\psi, \tag{16}$$

where $\mu = \cos \vartheta$, ψ is the observation azimuth angle, ϑ is the observation zenith angle, $R(\mu, \mu_0, \psi)$ is the reflection function of the layer, and $T(\mu, \mu_0, \psi)$ is the transmission function of the layer [13,14].

For nonabsorbing particles, the equations of Table 5 can be simplified:

$$R(\mu_0) = 1 - T(\mu_0), \qquad T(\mu_0) = TK_0(\mu_0), \tag{17}$$

Table 5
Radiative characteristics of weakly absorbing, optically thick layers [14,21] ($y = 4s$, $s = 4\sqrt{(1-\omega_0)/3(1-g)}$, $z = \frac{3}{4}(1-g)\tau$, $K_0(\mu_0) = \frac{3}{7}(1 + 2\mu_0)$)

Radiative characteristic	Formula
Absorptance A	$1 - \dfrac{\sinh(y) + \sinh(yz)}{\sinh((1+z)y)}$
Plane albedo $R(\mu_0)$	$\exp(-yK_0(\mu_0)) - TK_0(\mu_0)\exp(-(1+z)y)$
Spherical albedo R	$\dfrac{\sinh(yz)}{\sinh((1+z)y)}$
Transmittance $T(\mu_0)$	$TK_0(\mu_0)$
Global transmittance T	$\dfrac{\sinh(y)}{\sinh((1+z)y)}$

and

$$R = \frac{z}{1+z}, \qquad T = \frac{1}{1+z}, \tag{18}$$

where

$$z = \tfrac{3}{4}\tau(1-g). \tag{19}$$

According to Table 4, spherical particles have the smallest values of $1-g$ (and z). Thus, the global transmittance of light by layers consisting of nonabsorbing nonspherical particles T_n is lower [see Eq. (18)] than the global transmittance T_s in the case of layers with spherical particles assuming the same τ. The relative differences are

$$\frac{T_s - T_n}{T_s} = \frac{0.75\tau(g_s - g_n)}{1 + 0.75\tau(1-g_n)} > 0, \tag{20}$$

where g_s and g_n denote the asymmetry parameters for spherical and nonspherical particles, respectively. Correspondingly, the reflection of light by nonabsorbing layers consisting of nonspherical particles R_n is greater than the reflection R_s by layers of spheres:

$$\frac{R_s - R_n}{R_s} = \frac{g_n - g_s}{(1 + 0.75\tau(1-g_n))(1-g_s)} < 0. \tag{21}$$

This qualitative behaviour also holds for weakly absorbing semi-infinite light scattering media. From Table 5 as $\tau \to \infty$, it follows that

$$R_\infty(\mu_0) = \exp(-yK_0(\mu_0)), \qquad R_\infty = \exp(-y), \qquad y = 4s, \tag{22}$$

where R_∞ and $R_\infty(\mu_0)$ are the spherical and the plane albedos of a semi-infinite layer. As expected, the transmittance is equal to zero at $\tau \to \infty$. Again, with $y = 4s$ being the largest for spheres (see Table 4), it follows that $R_{s,\infty} < R_{n,\infty}$, where symbols n and s denote nonspherical and spherical scatterers, respectively.

Increasing the particle nonsphericity produces the same effect on the radiative fluxes as decreasing their size. Smaller particles imply smaller absorption and larger reflection. For the solution of the inverse problem in the case of disperse media consisting of weakly absorbing nonspherical particles (e.g., snow [22–24]) it follows that the approximation of spherical particles will underestimate the particle size. This underestimation is often related to the presence of pollutants in snow (e.g., soot, dust, heavy metals, etc.). It is interesting to note that the parameter y is proportional to both the degree of particle nonsphericity and the concentration of pollutants. Indeed, the value of y is determined by

$$y = 4\sqrt{\frac{1-\omega_0}{3(1-g)}}, \tag{23}$$

where $1-\omega_0 = \sigma_{abs}/\sigma_{ext}$. The extinction coefficient is determined by Eq. (12). The absorption coefficient of a large, weakly absorbing particle can be approximated by $\sigma_{abs} = f\gamma c$, where $\gamma = 4\pi\chi/\lambda$

and f is the shape parameter [7]. We then have

$$y = N\sqrt{\gamma a_{\mathrm{ef}}}, \tag{24}$$

where the parameter

$$N = \frac{4}{3}\sqrt{\frac{2f}{(1-g)}} \tag{25}$$

depends on the particle shape. Thus, the accuracy of the values of a_{ef} retrieved from the value of $y = \ln(R_\infty^{-1})$ depends, according to Eq. (24), on the assumed value of $N\sqrt{\gamma}$:

$$a_{\mathrm{ef}} = \frac{y^2}{\gamma N^2}. \tag{26}$$

Therefore, low values of a_{ef} as compared to in situ measurements may be explained by the fact that the true absorption coefficient and/or the true value of N are larger than those used in the retrieval procedure.

It follows from Table 4 that N is always larger for nonspherical particles than for spheres. Note, that this important parameter can be found from Eq. (26) if the effective radius is available from independent in situ measurements:

$$N = \frac{y}{\sqrt{\gamma a_{\mathrm{ef}}}}. \tag{27}$$

Let us consider the absorptance $A = 1 - R - T$ now. It follows for small values of y (see Table 5) that

$$A = 2\tau_{\mathrm{a}}, \tag{28}$$

where $\tau_{\mathrm{a}} = \sigma_{\mathrm{abs}} l$ is the optical thickness due to absorption of light by particles. The value of $\sigma_{\mathrm{abs}} = (1 - \omega_0)\sigma_{\mathrm{ext}}$ is smaller for spheres (see Table 4). Thus, the absorptance of light by layers with nonspherical particles is higher when $y \to 0$.

Figs. 2 and 3 show the results for R, T, and A at $\lambda = 0.645$ and 1.24 μm based on the formulas presented in Table 5 and the data from Table 4. As expected [12], the differences in $T(\tau)$ and $R(\tau)$ for different shapes generally decrease with increasing optical thickness, being smaller for smaller absorption. This can be explained by the fact that photons in semi-infinite media are highly randomized and the shape of particles is not so important as in the case of thinner layers.

The absorptance A is most sensitive to the particle shape. Layers with spherical particles absorb less radiation than layers with nonspherical particles at small y. This is related to the fact that A is proportional to the absorption coefficient σ_{abs} at small values of y [see Eq. (28)]. However, for $\tau \to \infty$, we have [see Eq. (22)]

$$A = 1 - \exp(-y). \tag{29}$$

It follows that regardless of the fact that the absorption coefficient of spherical scatterers is smaller, the absorptance of the radiation in a semi-infinite layer with spherical particles

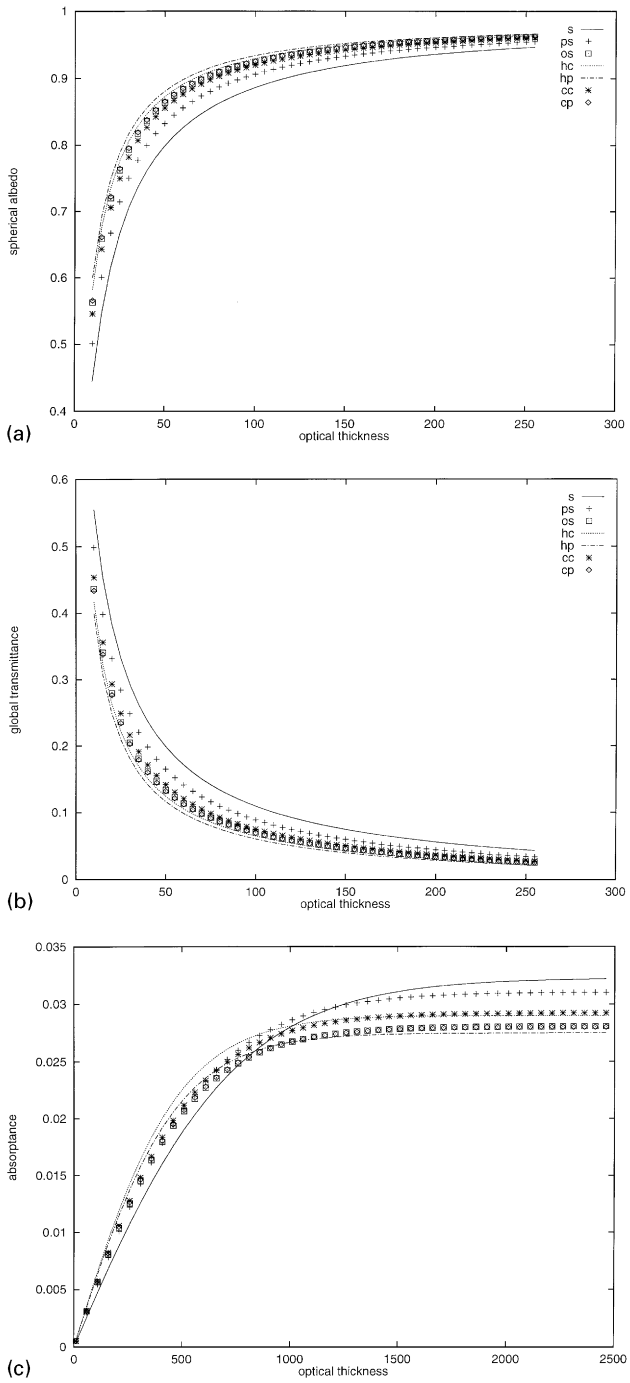

Fig. 2. Dependence of the spherical albedo (*a*), global transmittance (*b*), and absorptance (*c*) for layers with different types of particles (s — spheres, ps — prolate spheroids, os — oblate spheroids, hc — hexagonal cylinders, hp — hexagonal plates, cc — circular cylinders, cp — cicular plates) on the optical thickness at a wavelength of $\lambda = 0.645$ μm.

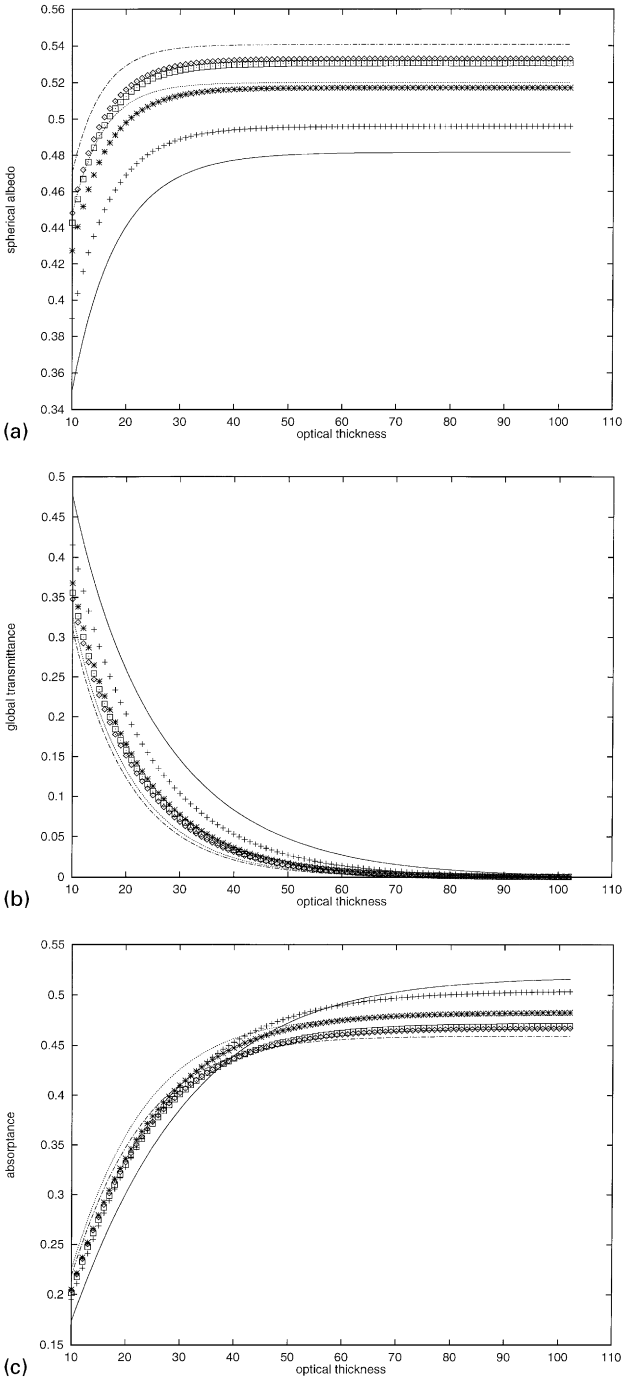

Fig. 3. As in Fig. 2, but for $\lambda = 1.24\ \mu m$.

is higher than in case of layers with nonspherical scatterers. This is because $y = 4s$ for spheres is the largest among all particles under consideration (see Table 4). Thus, semi-infinite layers with spherical particles absorb more radiation than semi-infinite media with nonspherical particles having the same effective radius. This result is due to the larger asymmetry parameter for spheres, which allows photons to penetrate into deeper layers and be trapped there.

Opposite signs of the albedo difference $\Xi = A_s - A_n$ (A_s and A_n are the absorptances of layers with spherical and nonspherical particles, respectively), at small and large thicknesses imply that there is a certain value of $\tau = \tau_0$ where $\Xi = 0$. Note that τ_0 depends on the particle shape (see Figs. 2c and 3c).

It follows from Figs. 2 and 3 that weakly absorbing thick layers with spherical particles appear darker (smaller values of R) than layers with nonspherical particles with the same volume/surface ratio and concentration. They are also more transparent (larger values of T). This agrees with results for nonabsorbing layers [see Eqs. (20) and (21)]. Results for elongated and flattened particles of the same type (cylinders, hexagonal particles) are very close. In all cases the radiative fluxes for prolate spheroids are closest to those for spheres. On the other hand, differences in R, T and A are most pronounced for spheres and hexagonal columns.

4. Conclusion

It is a well-known fact that bidirectional reflection and transmission functions of turbid layers consisting of nonspherical particles strongly depend on their shape [8–12,25]. The same is true for their polarization characteristics.

However, it is sometimes believed that the difference between integral radiative characteristics for particles of different shapes is averaged out by multiple scattering. This is indeed the case for small (compared to the wavelength of the incident radiation) particles (see Fig. 1). In this case, nonspherical particles can be substituted by volume-equivalent spheres. However, for large particles the difference between different shapes of scatterers must be taken into account.

We investigated the special case of weakly absorbing, optically thick ($\tau > 7$) layers with particles of different shapes. It was found that semi-infinite, weakly absorbing turbid media consisting of spherical particles are characterized by smaller spherical albedos R and larger absorptances A compared to layers with nonspherical particles with shape parameters smaller than 4 and $a_{ef} = const$. It is interesting to note that these differences are smaller for randomly oriented infinite circular cylinders [26].

The absorptance of light at small values of τ_a ($y \to 0$) is smaller in the case of media consisting of spherical particles (see Figs. 2c and 3c). The transmittance of light through finite layers with spherical particles is higher than in the case of layers with nonspherical particles. Taking into account different incidence angles (see Table 5) does not change our conclusions.

Differences between phase functions, single scattering albedos, and asymmetry parameters of spheres and randomly oriented convex nonspherical particles gradually disappear with increasing absorption [17,27]. In this limit the model of equivalent spheres is indeed appropriate. This factor

simplifies all calculations at large absorption and can be used, e.g., in the spectroscopy of turbid media with large, strongly absorbing nonspherical particles [5].

Acknowledgements

The authors are grateful to M.I. Mishchenko for discussions and help. A.A.K. held an Alexander von Humboldt Fellowship during the course of this research. He thanks Prof. R. Weichert for his support and important advice.

References

[1] Lacis AA, Mishchenko MI. Climate forcing, climate sensitivity, and climate response: a radiative modeling perspective on atmospheric aerosols. In: Charlson RJ, Heintzenberg J, editors. Aerosol forcing of climate. New York: Wiley, p. 11–42.
[2] de Haan JF. Effects of aerosols on the brightness and polarization of cloudless planetary atmospheres. Ph.D. thesis, Free University, Amsterdam, 1987. p. 150–3.
[3] Macke A, Mishchenko MI. Appl Opt 1996;35:4291–6.
[4] Mühlenweg H, Hirleman ED. The influence of particle shape on diffraction spectroscopy. In: Weichert R, editor. Proceedings of the Seventh European Symposium on Particle Characterization, vol. 1. Nurnberg Messe GmbH, 1998. p. 181–90.
[5] Kokhanovsky AA, Determination of the refractive index of large strongly absorbing particles under multiple light scattering conditions. In: Weichert R, editor. Proceedings of the Seventh European Symposium on Particle Characterization, vol. 2. Nurnberg Messe GmbH, 1998. p. 517–26.
[6] Takano Y, Liou K-N. J Atmos Sci 1989;46:3–19.
[7] Kokhanovsky AA, Macke A. Appl Opt 1997;36:8785–90.
[8] Kinne S, Liou K-N. Atmos Res 1989;24:273–84.
[9] Minnis P, Liou K-N, Takano Y. J Atmos Sci 1993;50:1279–304.
[10] Liou K-N, Takano Y. Atmos Res 1994;31:271–98.
[11] Mishchenko MI, Rossow WB, Macke A, Lacis AA. J Geophys Res 1996;101:16973–85.
[12] Chervet P, Isaka H, Nakajima T. Ann Geophys 1996;14:837–44.
[13] Sobolev VV. Light scattering in planetary atmospheres. Moscow: Nauka, 1972.
[14] Kokhanovsky AA, Nakajima T, Zege EP. Appl Opt 1998;37:4750–7.
[15] Macke A. Modellierung der optischen Eigenschafte von Cirruswolken. Ph.D. thesis, GKSS-Forschungszentrum Geesthacht GmbH, Geesthacht, 1994. p. 19–66.
[16] Macke A, Mueller J, Raschke E. J Atmos Sci 1996;53:2813–25.
[17] van de Hulst HC. Light scattering by small particles. New York: Dover, 1981.
[18] Huffman DR, Bohren CF. Infrared absorption spectra of non-spherical particles treated in the Rayleigh-ellipsoid approximation. In: Schuerman DW, editor. Proceedings of the International Workshop on Light Scattering by Irregularly Shaped Particles. New York: Plenum Press, 1980. p. 103–11.
[19] Bohren CF, Huffman DR. Absorption and scattering of light by small particles. New York: Wiley, 1983.
[20] Yang P, Liou KN. Contr Atmos Phys 1998;71:223–48.
[21] Zege EP, Ivanov AP, Katsev IL. Image transfer through a scattering medium. Berlin: Springer, 1991.
[22] Fily M, et al. Remote Sens Environ 1997;59:452–60.
[23] Warren SG. Rev Geophys Space Phys 1982;20:67–89.
[24] Zege EP et al. The retrieval of the effective radius of snow grains and control of snow pollution with GLI data. In: Mishchenko MI, Travis LD, Hovenier JW, editors. Conference on Light Scattering by Nonspherical Particles: Theory, Measurements, and Applications, Boston, MA, USA: American Meteorological Society, 1998. p. 288–90.

[25] Nakajima TY, Kokhanovsky AA, Nakajima T. Global analysis of ice clouds: Accounting for the nonspherical effects. In: Mishchenko MI, Travis LD, Hovenier JW, editors. Conference on Light Scattering by Nonspherical Particles: Theory, Measurements, and Applications, Boston, MA, USA: American Meteorological Society, 1998. p. 301–4.
[26] Grenfell T, Warren S. Representation of a nonspherical ice particle by an assembly of spheres. In: Mishchenko MI, Travis LD, Hovenier JW, editors. Conference on Light Scattering by Nonspherical Particles: Theory, Measurements, and Applications, Boston, MA, USA: American Meteorological Society, 1998. p. 51–4.
[27] Kokhanovsky AA. Optics of light scattering media: problems and solutions. Chichester: Wiley-Praxis, 1999.